CHEMICAL PHYSICS

How volatile components catalyze vapor nucleation

Chenxi Li[1,2], Jan Krohn[2], Martina Lippe[2], Ruth Signorell[2]*

Gas phase nucleation is a ubiquitous phenomenon in planetary atmospheres and technical processes, yet our understanding of it is far from complete. In particular, the enhancement of nucleation by the addition of a more volatile, weakly interacting gaseous species to a nucleating vapor has escaped molecular-level experimental investigation. Here, we use a specially designed experiment to directly measure the chemical composition and the concentration of nucleating clusters in various binary CO_2-containing vapors. Our analysis suggests that CO_2 essentially catalyzes nucleation of the low vapor pressure component through the formation of transient, heteromolecular clusters and thus provides alternative pathways for nucleation to proceed more efficiently. This work opens up new avenues for the quantitative assessment of nucleation mechanisms involving transient species in multicomponent vapors.

Copyright © 2021 The Authors, some rights reserved; exclusive licensee American Association for the Advancement of Science. No claim to original U.S. Government Works. Distributed under a Creative Commons Attribution NonCommercial License 4.0 (CC BY-NC).

INTRODUCTION

Gas-phase nucleation is the very first step of a vapor's transition to the condensed phase, taking a critical role in the formation of cloud condensation nuclei (*1*, *2*), various industrial processes (*3*, *4*), and stardust formation (*5*). It has been observed that the introduction of a second, high vapor pressure gas can markedly increase the nucleation rate of another vapor (*6*, *7*). For instance, sulfuric acid is widely recognized as a major precursor in atmospheric new particle formation (NPF), but its unary nucleation rate is too low to explain the observed NPF rates (*8*). Realistic estimates of NPF rates must account for the enhancing effect of water, organic compounds, and ammonia/amines on sulfuric acid nucleation (*1*, *9*–*13*).

Unravelling the mechanism of the enhancing effect requires the experimental determination of the molecular composition of the clusters initially formed in the nucleation process (nucleating clusters) and the quantitative tracing of their concentration. In general, this is a challenging task (*14*) because the nucleating clusters are delicate entities—even in mass spectrometric studies, they often escape detection as they are easily altered or even destructed upon ionization and during transport (*15*, *16*). Recent developments in mass spectrometry made it possible to identify at least the relatively strongly bound constituents in the nucleating clusters (*17*, *18*), such as sulfuric acid, amines, or highly oxidized molecules. While this has provided remarkable details about the initial steps of atmospheric NPF (*1*, *9*, *19*), the measurements remained blind to the species that exhibit weaker interactions (weakly interacting species) in the nucleating clusters. Because they easily evaporate, weakly bound constituents of nucleating clusters have so far eluded detection. Water is a notable example. Despite its tendency to form hydrogen bonds, it is mostly missing from the mass spectra recorded during NPF events, even though humidity is known to influence nucleation rates (*1*, *20*, *21*).

To understand the role of weakly interacting species in nucleation, experimental approaches are required that initiate nucleation under well-controlled conditions, preserve the integrity of the nucleating clusters, and quantify their number concentrations with high accuracy, to enable a data-based kinetic analysis. A new nucleation instrument recently developed in our group is designed to meet these requirements (*22*–*24*): The postnozzle flow of a Laval expansion creates a nucleation region with uniform temperature and pressure (*22*, *25*, *26*), while coupling to mass spectrometry by ultrasoft, single-photon ionization in vacuo minimizes cluster fragmentation upon detection to the lowest level nowadays achievable (*27*, *28*). This instrument is capable of quantifying the number concentrations of weakly bound nucleating clusters and providing time-dependent, molecular-level information on their size and chemical composition. This instrument has already revealed unprecedented molecular-level details on unary nucleation dynamics (*22*–*24*, *29*–*31*), which predestines it for extended investigations of more complex binary/multicomponent nucleation events.

The present study reports molecular-level observations of the nucleation enhancement by weakly interacting species in binary vapors. With the important role of CO_2 nucleation in the Martian atmosphere (*32*–*34*) and the potential use of CO_2 for carbon capture and storage (*35*) in mind, we have selected various model systems containing CO_2 as the nucleation-enhancing species in binary vapors. On the basis of a detailed kinetic analysis, we quantitatively discuss the participation of CO_2 in the cluster formation process, demonstrating that CO_2 essentially functions as a catalyst to enhance nucleation. By covering a broad temperature range, we show that the ability of CO_2 to enhance nucleation decreases with increasing temperature. The general implications of our current work are discussed in relation to previous nucleation studies.

RESULTS

Nucleation in the postnozzle flow of a Laval expansion

Figure 1 illustrates the experimental setup (*22*, *25*). Nucleating vapors along with a carrier gas (argon, nitrogen, or mixtures) are supplied to the stagnation volume of a Laval nozzle [red shaded area (*36*–*38*), at temperature T_0 and pressure p_0]. As the gas mixture expands through the nozzle, the temperature drops quickly, leading to supersaturation of the nucleating vapors. The unique features of our experiment are the initiation and observation of the nucleation in the uniform postnozzle flow [blue shaded area; this flow uniformity has previously been exploited in studies of chemical kinetics (*37*–*43*)], and the online retrieval of molecular information about the composition of the molecular clusters. The postnozzle flow acts

[1]School of Environmental Science and Engineering, Shanghai Jiao Tong University, Shanghai 200240, China. [2]Department of Chemistry and Applied Biosciences, Laboratory of Physical Chemistry, ETH Zürich, Vladimir-Prelog-Weg 2, CH-8093 Zürich, Switzerland.
*Corresponding author. Email: rsignorell@ethz.ch

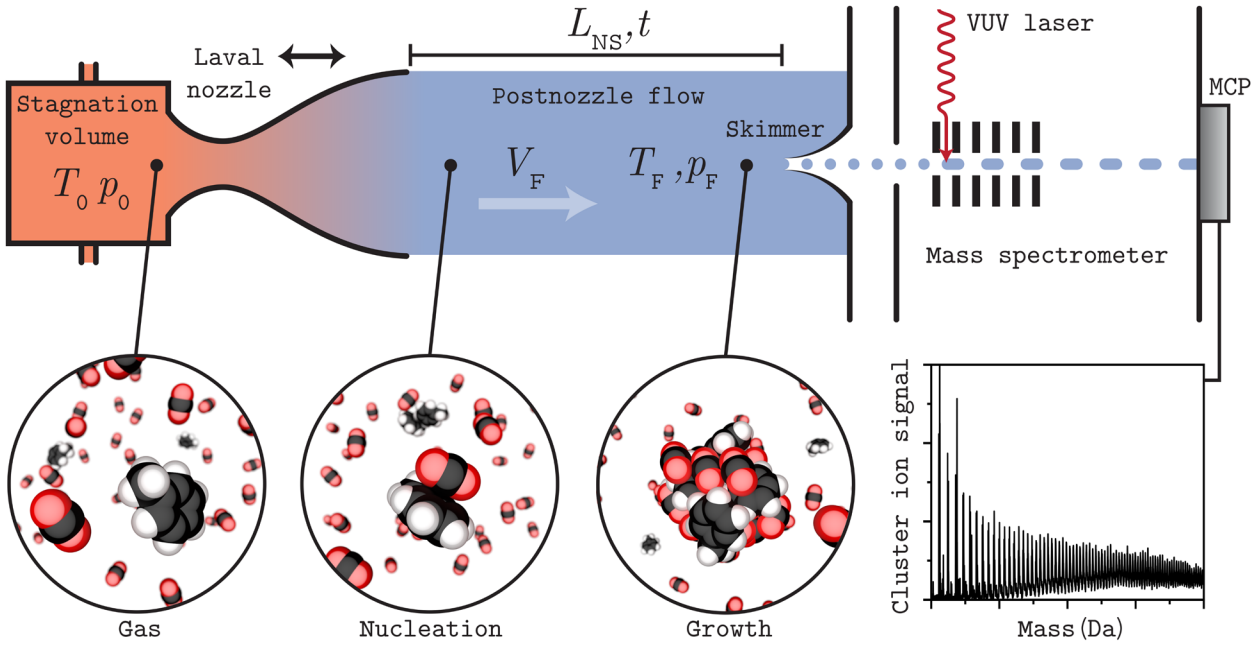

Fig. 1. Illustration of the experimental setup and the nucleation process. The four inset plots show (from left to right) free vapor molecules in the stagnation volume, the onset of nucleation, a cluster after some growth, and an example mass spectrum of such grown clusters (right). The cluster ions are accelerated by the electrostatic lens and detected by a microchannel plate detector (MCP).

as a flow reactor without walls, allowing us to study nucleation under uniquely well-controlled conditions (constant velocity V_F, flow temperature T_F, flow pressure p_F, and saturation ratio S; see Materials and Methods for details of flow temperature adjustment), a crucial prerequisite for nucleation experiments because nucleation is exquisitely sensitive to changes in conditions. The mass of the molecular clusters is probed with time-of-flight mass spectrometry directly in vacuo after soft ionization with a vacuum ultraviolet (VUV) laser at a photon energy of 13.8 eV (*27*, *28*, *44*, *45*). In this way, the detection largely keeps the clusters intact (*23*, *24*), so that their mass provides direct molecular-level information about their chemical composition and their size (number of molecules).

Different parts of the postnozzle flow can be probed by changing the nozzle exit–to–skimmer distance, L_{NS} (Fig. 1). L_{NS} can be modified in steps as small as 1 mm over a maximum length of ~10 cm, corresponding to steps of ~2 μs in the nucleation time t up to a maximum of ~200 μs. The onset of nucleation occurs at short L_{NS}, i.e., short t, where the first molecular clusters appear in the mass spectra ("Nucleation," Fig. 1). With increasing L_{NS} and thus t, the nucleated clusters continue to grow by vapor condensation ("Growth," Fig. 1).

Nucleation enhancement by a second vapor component

We start the discussion with an exemplary binary nucleation experiment carried out for a toluene-CO_2 mixture at $T_F = 55$ K. While the binary vapor undergoes nucleation and cluster growth (Fig. 2), neither toluene (toluene-only, red trace) nor CO_2 can nucleate on their own at the same vapor concentration and conditions. Figure 2A exemplifies this for the mass spectra recorded at the longest nucleation time at $L_{NS} = 100$ mm ($t \sim 200$ μs). Even at this point, when the binary mixture (yellow trace) has already nucleated and started to grow, no cluster signal shows up in the corresponding mass spectrum for pure toluene (toluene-only, red trace). Evidently, the presence of CO_2, although more volatile than toluene, greatly enhances toluene nucleation.

To understand the mechanism, we examine the composition of the very first clusters formed in the nucleation process of the binary mixture, which sets in at L_{NS} ~30 mm ($t \sim 60$ μs). Figure 2B shows a zoomed-in segment of the mass spectrum recorded at $L_{NS} = 40$ mm, i.e., right after the onset of nucleation. We only find cluster signals with mass-to-charge ratios (m/z) that are multiples of the singly ionized toluene molecules ($m/z = 92$). This means that the only detected nucleating clusters at $T_F = 55$ K are homo-molecular toluene clusters [$(Tol)_j$]. Given, however, the observed strong enhancement of nucleation by the presence of CO_2, mixed CO_2-containing clusters [$(Tol)_j(CO_2)_{x>0}$] must be involved in the nucleation process. Such mixed clusters can indeed be detected at lower temperatures of 31 K (see the "Effect of temperature" section below). So why are they not observed at 55 K? One reason could be that they are losing CO_2 (evaporation) on their way to the ionization point, implying a lifetime of <500 μs (the traveling time of the clusters from the skimmer to the ionization point). This could indicate that equilibration through collisions with the carrier gas molecules is too slow at the low flow pressure of our experiments, so that a certain amount of excess energy (i.e., exceeding the thermal energy) remains in the mixed clusters after their formation. The fact that whole series of $(Tol)_j(CO_2)_{x>0}$ are detected at lower flow temperatures (see the "Effect of temperature" section below) indicates that such incomplete thermalization is not the only factor. Rather, these observations provide a hint that the mixed clusters play the role of transient species in the nucleation mechanism itself. This provides the basis for the kinetic scheme we propose in the "Kinetic modeling" section.

The above discussion refers to the initial nucleation step. This is followed later on by the growth of the clusters that were formed in the nucleation step. At the later stages of this growth process, CO_2 starts to condense on the preformed clusters as evidenced by the

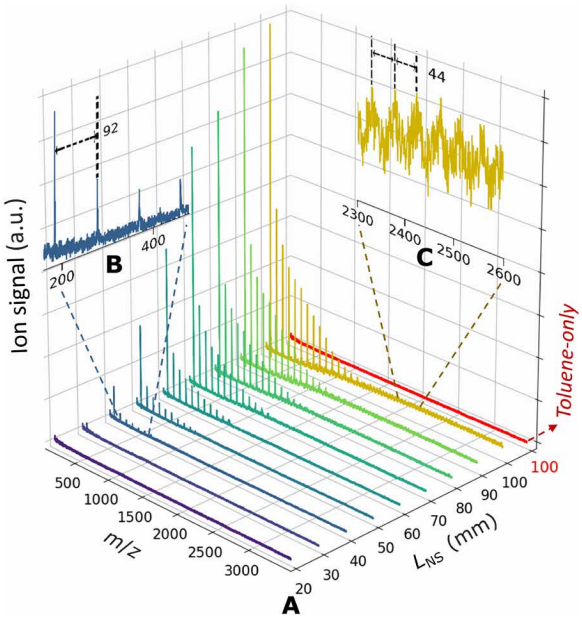

Fig. 2. An example of nucleation enhancement of toluene by CO_2. (**A**) Mass spectra for binary toluene-CO_2 nucleation as a function of L_{NS} (equivalently, nucleation time *t*) recorded at T_F = 55 K and p_F = 40 Pa for a toluene concentration of 1.73 × 10^{13} cm^{-3} and a CO_2 concentration of 5.55 × 10^{14} cm^{-3} (CT4 in table S1). The red mass spectrum is a reference spectrum measured at L_{NS} = 100 mm for the same toluene concentration but without CO_2 in the flow ("toluene-only"). (**B** and **C**) Zoomed-in segments of the mass spectra for binary nucleation recorded at L_{NS} = 40 and 100 mm, respectively. *m/z* is the dimensionless mass-to-charge ratio. a.u., arbitrary units.

mass spectra observed at longer times *t*. An example is shown in Fig. 2C for a zoomed-in segment of the mass spectrum at L_{NS} = 100 mm (t ~ 200 μs). The *m/z* difference of 44 between neighboring cluster signals indicates that CO_2 condensation is becoming a major driving force of cluster growth at this stage.

Kinetic modeling

To gain further insight into the role of CO_2 in the nucleation process, we have performed experiments at the same constant T_F = 55 K and p_F = 40 Pa as in Fig. 2, but for varying toluene and CO_2 concentrations (see conditions in table S1). The number concentrations N_j of clusters $(Tol)_j(CO_2)_x$ (referred to as "*j*-mers") are determined as a function of L_{NS} (see Materials and Methods). Conversion of L_{NS} to nucleation times *t* yields the temporal evolution of N_j (Fig. 3A shows examples for *j* = 2 to 6). For *j* = 2 to 6, the mass spectra show predominantly homo-molecular clusters (x = 0), similar to Fig. 2A, while hetero-molecular clusters (x > 0) are not directly observable under these conditions (T_F = 55 K).

From the N_j, we derive experimental rate constants $k_{1,j}$ for the association of toluene monomer with the *j*-mers (section S2). The ratio to a corresponding gas-kinetic hard sphere collision rate constant, $k_{1,j,hs}$ (section S2), defines the enhancement factor $\eta_{exp,j}$ (*29*)

$$\eta_{exp,j} = \frac{k_{1,j}}{k_{1,j,hs}} \quad (1)$$

Its value indicates how much faster the association of a toluene monomer with a *j*-mer proceeds in the actual experiment ($k_{1,j}$) compared with hard-sphere collisions [$k_{1,j,hs}$, calculated within standard gas kinetic theory (*46*) assuming bulk properties (*47*)] between toluene monomer and homo-molecular toluene clusters (section S2). By definition, $k_{1,j,hs}$ is independent of the CO_2 content, so that variations of $\eta_{exp,j}$ with the CO_2 concentration show how CO_2 affects the toluene monomer-*j*-mer association. Figure 3B shows the resulting $\eta_{exp,j}$ as a function of the CO_2 concentration for *j* = 2 to 6. To observe unary toluene nucleation (no CO_2) under the chosen conditions, we increased the toluene concentration 3.5 times compared with Fig. 2 (where no unary toluene nucleation was observed). $\eta_{exp,j=2-6}$ varies between ~2 and 5 for unary toluene nucleation, in qualitative agreement with our previous unary nucleation studies on water, CO_2, and propane (*29*, *31*). This range of enhancement factor is likely the result of intermolecular interactions between the colliding toluene monomer and the homo-molecular toluene clusters (*48*), which are not accounted for by $k_{1,j,hs}$. With increasing CO_2 concentration, $\eta_{exp,j}$ systematically increases for all *j* compared with unary nucleation, by up to a factor of ~4 for the highest CO_2 concentration of 8.3 × 10^{14} cm^{-3} (Fig. 3B). The dependence of $\eta_{exp,j}$ on the CO_2 concentration indicates the direct involvement of CO_2 in the formation of nucleating toluene clusters, suggesting that hetero-molecular $(Tol)_j(CO_2)_{x>0}$ clusters are essential, albeit transient species in the nucleation mechanism. Under the conditions in Fig. 2, where unary toluene nucleation does not occur, transient hetero-molecular clusters must even dominate the nucleation process.

Our previous study revealed dimerization as the rate-limiting step for unary toluene nucleation at 55 K (*23*). On the basis of this result and the above observations for binary nucleation, we propose the following models (R1 to R3)

$$Tol + Tol \xrightarrow{\alpha} (Tol)_2 \quad (R1)$$

$$CO_2 + Tol \xrightarrow{\beta} (Tol)(CO_2) \quad (R2)$$

$$(Tol)(CO_2) + (Tol)(CO_2)_x \xrightarrow{\gamma} (Tol)_2(CO_2)_y + (x - y + 1)\,CO_2 \quad \text{with } (x \le 1, y \le x + 1) \quad (R3)$$

where α, β, and γ are the rate constants of the respective reactions. R1 accounts for unary toluene nucleation and is ineffective at all our conditions, except for the experiment where we use a high toluene concentration and no CO_2 (unary case in Fig. 3; CT0 in table S1). R2 and R3 account for CO_2-toluene monomer interaction, postulating the formation of a transient cluster $(Tol)(CO_2)$ (R2) that precedes toluene dimerization (R3). The consecutive reactions R2 and R3 represent a CO_2-catalyzed toluene dimerization process. Catalytic clustering processes of weakly interacting species were previously hypothesized in free jet expansion experiments, e.g., to rationalize the increased HF dimer population observed in the presence of N_2O (*49*).

The proposed mechanism R1 to R3 is, to some extent, analogous to the chaperon or radical-complex mechanisms for radical recombination, where the direct recombination [analogous to (R1)] competes with a reaction of a radical monomer with a weakly bound preformed radical cluster (*50*–*53*). The latter is analogous to R3 for x, y = 0 and is typically invoked for radical recombinations of small molecules at low temperatures and higher densities. In our experiments, by contrast, the pressure is extremely low (total pressure, 40 Pa; involved active species, <1 Pa; table S1); with toluene, we already have a relatively large molecule (42 internal degrees of freedom), and the products are only weakly bound. It is thus an intriguing

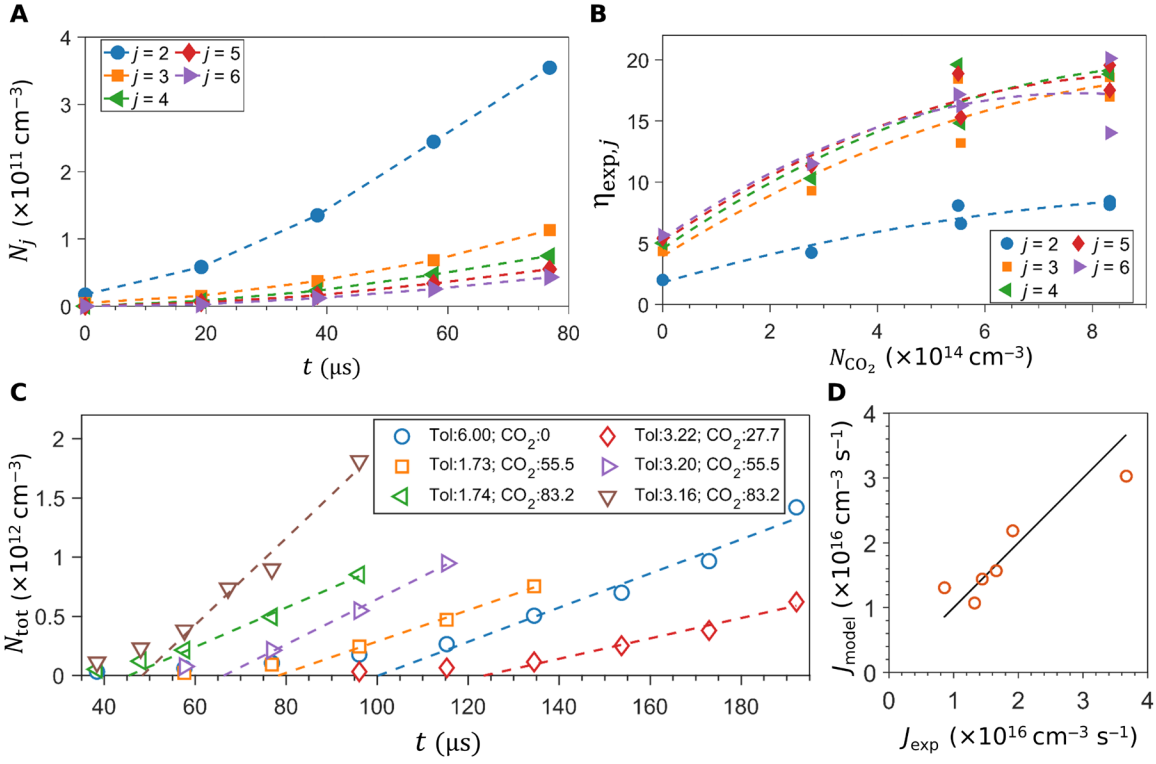

Fig. 3. Kinetic analysis of binary toluene-CO_2 nucleation at constant T_F = 55 K and p_F = 40 Pa. (**A**) Concentration N_j of the j-mers (j = 2 to 6) as a function of the nucleation time t. The toluene and CO_2 concentrations in the postnozzle flow are 1.73 × 10^{13} cm^{-3} and 5.55 × 10^{14} cm^{-3} (CT4 in table S1), respectively. (**B**) Enhancement factor $\eta_{exp,j}$ as a function of the CO_2 concentration N_{CO_2} for j = 2 to 6. Dashed lines are quadratic fits to the data points (symbols). (**C**) Total number of clusters N_{tot} as a function of t for six different toluene-CO_2 concentrations (CT0 to CT5; table S1). The legend shows the concentrations in units of 10^{13} cm^{-3}. The dashed lines are linear fits to the experimental data points (symbols). (**D**) Circles: Comparison of the experimental nucleation rates J_{exp} and the modeled nucleation rates J_{model} (Eq. 2). The straight black line is a reference line with a slope of 1.

result that such a mechanism turns out to be applicable to vapor nucleation. Our proposed mechanism differs in two aspects from the usual chaperon mechanism. We avoid the assumption of equilibrium for the formation of the chaperon cluster (R2), as equilibration might be too slow at the very low pressure conditions of our experiments. For simplicity, we describe this step with a single forward rate constant β, noting that this is only an effective rate constant. In addition to the usual chaperon mechanism, we also account for the reaction of two chaperon clusters (R3 for $x > 0$). While this contribution to the overall kinetics at 55 K is minor, it is necessary to account for the detection of a broad range of small CO_2-containing mixed clusters at lower temperatures (31 K in Fig. 4B), where at least a notable fraction of toluene is expected to be present in the form of Tol-CO_2 (see the "Effect of temperature" section; Fig. 4B).

In line with the experimental observations in Figs. 2 and 3, R3 is generally far more efficient than R1 in creating toluene dimers because extra CO_2 molecules can accommodate the excess collision energy, either by evaporation or by providing additional degrees of freedom. R3 is therefore assumed to be collision-limited. R1, R2, and R3 are incorporated into a kinetic model (section S3) that is simultaneously fitted to the time-dependent experimental cluster size distributions for all conditions recorded (CT0 to CT5 in table S1). We use β as a free fitting parameter, while α is determined from the unary toluene experiment (CT0), and γ is assumed to be equal to the collision rate constants of the reactants (section S3). Because R3 is not rate determining (γ ≫ β), the model yields the following simple expression for the nucleation rate

$$J_{model} = \alpha N_{Tol}^2 + \beta N_{Tol} N_{CO_2} \quad (2)$$

with α = 4 × 10^{-12} cm^3 s^{-1} and β = 1 × 10^{-12} cm^3 s^{-1} obtained from the fit to the experimental data (fig. S1). N_{Tol} and N_{CO_2} are the concentrations of toluene and CO_2 monomers, respectively. The first term arises from the bare dimerization, R1, while the second term accounts for the CO_2-assisted dimerization, R2 and R3, which is first order in both the toluene and the CO_2 concentration. The values of J_{model} are listed in table S1.Alternatively, experimental nucleation rates, J_{exp}, can be retrieved directly from the experimental spectra by taking the first-order derivative of total cluster concentration N_{tot} (Materials and Methods) with respect to the nucleation time (*24*, *54*)

$$J_{exp} = \frac{dN_{tot}}{dt} \quad (3)$$

Figure 3C shows N_{tot} as a function of the nucleation time t. The dashed lines are linear fits whose slopes correspond to J_{exp}. The values of J_{exp} are listed in table S1. Figure 3D compares J_{model} and J_{exp} on a linear scale illustrating the excellent agreement between the model fit and the experimentally determined rates. Because Eq. 2 describes the nucleation kinetics quantitatively, our simple model of CO_2-catalyzed nucleation (R1 to R3) appears to provide a reasonable

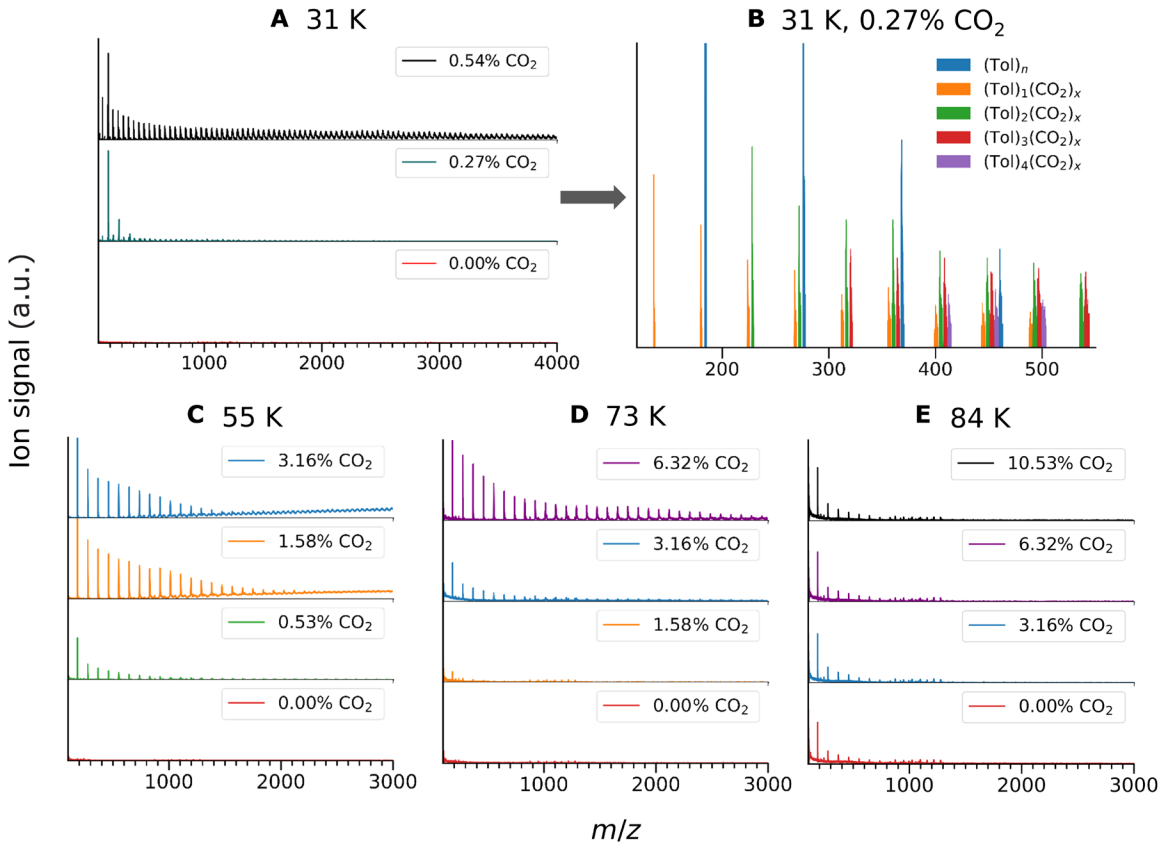

Fig. 4. Temperature dependence of binary toluene-CO_2 nucleation. The mass spectra are recorded at flow temperatures T_F of (**A** and **B**) 31 K, (**C**) 55 K, (**D**) 73 K, and (**E**) 84 K at a constant L_{NS} = 100 mm and for constant toluene concentrations. (B) A zoomed-in segment of the mass spectrum in (A) for 0.27% CO_2. The color code indicates the composition of the $(Tol)_j(CO_2)_x$ clusters. Detailed experimental conditions are specified in table S2. The indicated temperatures are the postnozzle flow temperatures without CO_2 addition, rounded to the nearest integer.

representation of the underlying mechanism. In accordance with the simple two-parameter expression of Eq. 2, J_{exp} increases with increasing CO_2 concentration at approximately constant toluene concentration. J_{exp} likewise increases with increasing toluene concentration at constant CO_2 concentration. The proposed mechanism R1 to R3 seems to capture the essence of the nucleation process. More advanced direct simulations of the cluster formation processes (*26*, *55*), which could provide deeper insight, would be very challenging for the toluene-CO_2 system.

Effect of temperature

Figure 4 illustrates the influence of the temperature on binary nucleation in the temperature range T_F = 31 to 84 K. Except for T_F = 84 K, the toluene concentration was adjusted so that the onset of the unary toluene nucleation (0% CO_2) does just not yet occur at L_{NS} = 100 mm (bottom traces in Figs. 4, A to D). In the case of T_F = 84 K, where no enhancement by CO_2 is observed (see below), we adjusted the toluene concentration to obtain visible nucleation at L_{NS} = 100 mm (bottom trace in Fig. 4E; see table S2 for the vapor concentrations) to better visualize the trends. The influence of increasing amounts of CO_2 on the nucleation is shown in the middle and top traces in Fig. 4. It clearly shows that CO_2 enhances toluene nucleation compared with the unary case at all temperatures, except at the highest temperature of 84 K.

As discussed in the context of Figs. 2 and 3, the vast majority of clusters detected in the mass spectra at 55 K at the onset of nucleation are stable homo-molecular $(Tol)_j$ clusters. Initially formed (nucleating) hetero-molecular clusters $(Tol)_j(CO_2)_{x>0}$ dissipate part of their excess energy through the loss of CO_2 (R3). Those clusters that do not lose all CO_2 molecules directly after their formation (R3 for $y > 0$) are stabilized by collisions with the carrier gas. At the relatively low gas density (low pressure limit), the collisional deactivation is apparently not efficient enough to prevent complete loss of CO_2 from the clusters on their way to the ionization region. The same holds for the nucleating clusters at the higher temperatures. This behavior changes at the lowest temperature of 31 K (Fig. 4, A and B). In this case, a substantial amount of hetero-molecular $(Tol)_j(CO_2)_{x>0}$ clusters is observed in the region of the onset of nucleation (Fig. 4B). Two phenomena contribute to this effect. First, at lower temperature, the reduced collision energy means that less excess energy needs to be dissipated, and collisional deactivation by the carrier gas might also become more effective as the lifetime of the corresponding collision complexes increases. Second, at lower temperature, a larger fraction of toluene will be present in the form of Tol-CO_2. With an estimated binding energy on the order of 10 kJ/mol (*56*), the equilibrium ratio of Tol-CO_2 to Tol would change from a small fraction (less than a percent) at 55 K to a large excess of Tol-CO_2 at 31 K (see section S4). Even if the equilibrium is not maintained at the very low flow pressure of our experiment, the probability of forming the chaperon cluster described by the effective forward rate constant β (R2) is expected to increase substantially. As a result, the

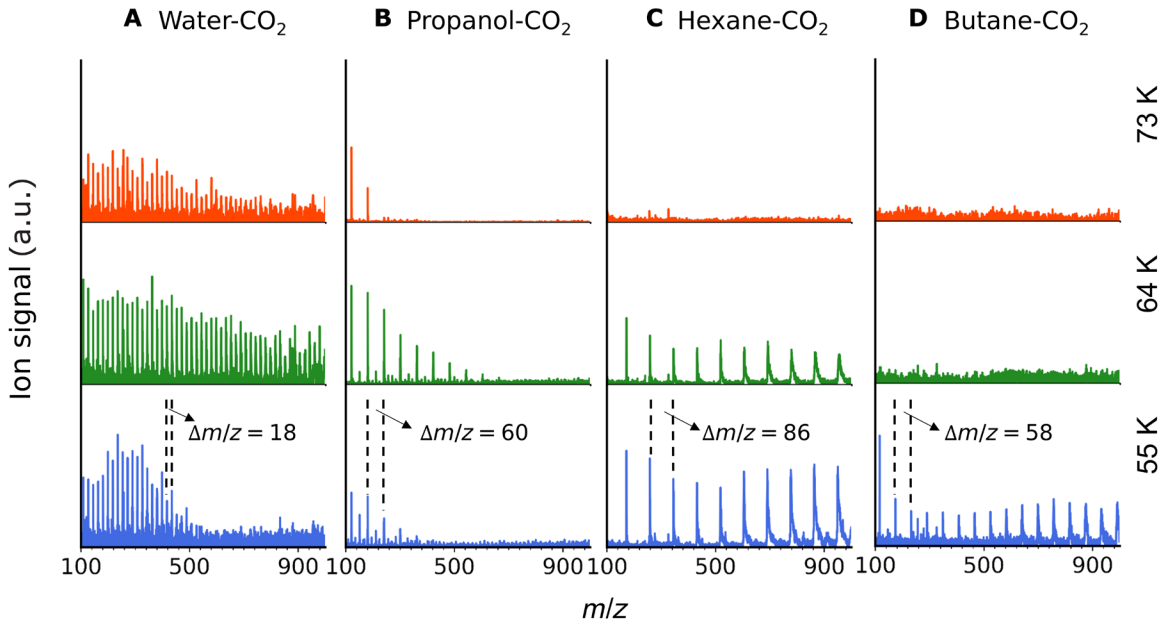

Fig. 5. Temperature dependence of the nucleation enhancement by CO_2 in several binary vapors (see also fig. S2). (**A**) Water-CO_2, (**B**) propanol-CO_2, (**C**) hexane-CO_2, and (**D**) butane-CO_2. The mass spectra are recorded at L_{NS} = 100 mm, a fixed CO_2 concentration of 3.16%, and a constant flow pressure of p_F = 40 Pa. The flow temperatures T_F are constant for each row, indicated on the right-hand side of the figure. The mass differences between neighboring peaks are indicated in spectra recorded at 55 K. They correspond to the molecular masses of water, propanol, hexane, and butane, respectively. Detailed experimental conditions are specified in table S3. The temperatures shown for each row are the postnozzle flow temperature without CO_2 addition, rounded to the nearest integer.

reaction of two chaperon clusters and thus the survival of CO_2 in hetero-molecular clusters becomes more likely (R3 with $x = 1$). By the same token, CO_2 becomes less effective in promoting nucleation as the temperature increases from 31 to 73 K. This is evidenced in the experiment by the increasing CO_2 concentrations required to enhance nucleation to a similar extent at rising temperatures (see Fig. 4, A, C, and D).

At 84 K (Fig. 4E), the enhancement effect by CO_2 is lost altogether, so that the mass spectra hardly change anymore with increasing CO_2 concentrations. At T_F = 84 K, CO_2 starts to behave like an inert carrier gas. Figure 4E demonstrates that both nucleation and growth become independent of the CO_2 content. CO_2 no longer enhances the nucleation of toluene (compare, e.g., 0% with 3.16% CO_2), nor does it anymore contribute to growth by condensation onto the toluene clusters (compare, e.g., 0% with 10.53% CO_2). This is in marked contrast to the behavior at the lower temperatures when CO_2 not only enhances nucleation but also is mainly responsible for early cluster growth, as revealed by the mass spectra recorded at higher CO_2 concentrations in Fig. 4 (A to D) (see also Fig. 2C).

CO_2: A more general nucleation enhancer

Is the toluene-CO_2 system a special case or does CO_2 also act as a nucleation enhancer in other binary systems? To answer this question, we investigated various binary vapors containing CO_2 and water, propanol, hexane, and butane, respectively. Figure 5 and fig. S2 show the mass spectra sampled at L_{NS} = 100 mm for three different temperatures (55, 64, and 73 K) at a fixed CO_2 percentage of 3.16% of the total flow. For clarity, the mass range $m/z < 1000$ is shown in Fig. 5, while the spectra for the larger cluster masses ($m/z \geq 1000$) are displayed in fig. S2. Before CO_2 was introduced into the flow, we adjusted the concentrations of the second compounds so that the onset for unary nucleation is just about to occur right at the chosen distance of L_{NS} = 100 mm (not shown). The fact that the mass spectra after introduction of CO_2 show pronounced cluster peaks (Fig. 5 and fig. S2) indicates that CO_2 indeed enhances nucleation of all these rather different compounds. As found for toluene-CO_2 binary nucleation, an increase in temperature diminishes the enhancement effect. The extent of the temperature effect varies in the different binary mixtures. Butane-CO_2 and hexane-CO_2 nucleation no longer proceeds at 64 and 73 K, respectively, while water-CO_2 and propanol-CO_2 nucleation still continues at these higher temperatures. The different intermolecular interactions between CO_2 and the various second compounds provide a plausible explanation for this observation. Butane-CO_2 and hexane-CO_2 mostly interact through weak van der Waals forces, so that the probability of forming the transient hetero-molecular nucleating clusters (and with it the enhancement effect of CO_2) decreases more rapidly with rising temperature than in the case of the more strongly bound water-CO_2 and propanol-CO_2 systems (both induction and van der Waals interactions). As the system with the strongest intermolecular interactions in the series, water-CO_2 nucleation is expected to be the least temperature sensitive. The mass spectra in Fig. 5 confirm this expectation. They also reveal that most of the smaller clusters are homo-molecular (i.e., without CO_2), which is consistent with the above observations for the binary toluene-CO_2 system (Fig. 2): At temperatures at and above ~55 K, the nucleating hetero-molecular clusters responsible for the nucleation enhancement (R2 and R3) lose their CO_2 on the time scale of the detection (see the previous section).

The temperature trend shown in Fig. 5 is qualitatively consistent with previous binary nucleation studies for hexane-CO_2 and water-CO_2 in supersonic nozzles by Wyslouzil and co-workers (*57*, *58*). Even though these studies did not provide molecular-level information on nucleating clusters, they show that the addition of CO_2 to nucleating water or hexane vapors does not affect the onset of water nucleation at

~200 K or hexane nucleation in the temperature range of 127 to 148 K. This agrees with the trend we observe in Fig. 5: With rising temperature, hexane-CO_2 and water-CO_2 interactions become increasingly ineffective to initiate nucleation pathways such as R2 and R3.

DISCUSSION

With molecular-level details, we have shown that transient, heteromolecular clusters provide the key to explain enhanced nucleation rates in CO_2-containing binary vapors. Through the intermediate formation of those clusters, CO_2 catalyzes the nucleation of the lower vapor pressure components. This marks an important step in unravelling the mechanisms of vapor nucleation because such weak interactions between a nucleation enhancer (CO_2) and another vapor component previously escaped time-resolved, molecular-level observations. Our work also serves as an integral part in understanding the nucleation phenomenon across different temperature regimes: In atmospheric NPF studies, it is established that acid-base reactions and strong hydrogen bonds (*6*, *59*) play an important role in promoting nucleation at ambient temperatures. The present study reveals that this role is taken by weak intermolecular interactions, such as van der Waals and dipole-induced dipole interactions, as temperature decreases. This result has further implications for the parametrization of nucleation rates for multicomponent vapors, as it indicates that with changing temperature, the type and number of species involved in the nucleation process also have to be adjusted properly. The temperature acts as a sensitive control for the nucleation mechanism, turning on and off different nucleation pathways involving different species (*1*). This could be particularly important in the modeling of atmospheric NPF events involving organics as different organic compounds likely enter the nucleation and particle growth processes at different temperatures (*60*), depending on their interaction strength with the other vapor components.

MATERIALS AND METHODS

Temperature control

To adjust the flow temperature in coarse and fine steps, we use two methods based on gas dynamics. First, for a given carrier gas composition, the degree of gas expansion through the nozzle determines the postnozzle flow temperature. We can therefore change the flow temperature by using Laval nozzles with different physical dimensions. This method is used to change the flow temperature in large steps. Second, for a given Laval nozzle, the heat capacity ratio of the carrier gas influences the degree of cooling. In this study, we use mixtures of nitrogen and argon, which have different heat capacity ratios (1.40 and 1.67, respectively, at room temperature). Raising the nitrogen-to-argon ratio increases the postnozzle flow temperature, which we exploit to fine-tune the flow temperature by changing the carrier gas composition (*24*, *31*). Tables S1 to S3 specify the gas compositions for experiments shown in Figs. 3 to 5, respectively.

To minimize the temperature disturbance of the postnozzle flow upon the addition of CO_2, we simultaneously reduced the nitrogen content in the carrier gas by the same amount. Here, we make use of the fact that the heat capacity ratio of CO_2 becomes very similar to that of N_2 as the temperature drops below 100 K (*61*). In the most extreme case, i.e., 10% CO_2 at 84 K (top trace in Fig. 4E), we estimate that replacing N_2 by CO_2 increases the temperature by ~1.5 K to T_F = 85.1 K. Overall, for the traces presented in Figs. 4 and 5, the flow temperatures for varying CO_2 content lie within ±1.1 K of the temperatures specified in the figures.

Determination of cluster number concentration

A reference gaseous species (internal standard) of known number concentration N_s and known photoionization cross section σ_s is used for the determination of the absolute number concentrations of the clusters (j-mers), N_j. The internal standard is needed to properly account for instrumental variations between experiments, e.g., laser power fluctuations. N_j is derived from the following equation used in our previous work (*24*, *31*)

$$N_j = \frac{I_{\mathrm{Tol}}}{I_s}\frac{\sigma_s}{j \cdot \sigma_{\mathrm{Tol}}} \cdot N_s \quad (4)$$

I_{Tol} and I_s are the ion signals of the $(\mathrm{Tol})_j(\mathrm{CO_2})_x$ clusters and the internal standard, respectively, in the mass spectrum; σ_{Tol} is the molecular photoionization cross section of toluene. For the unary toluene nucleation experiments, methane is used as an internal standard. For the CO_2-containing binary nucleation experiments, CO_2 itself serves as the internal standard.

The total cluster concentration N_{tot} is calculated by the summation of all cluster concentrations from dimer to the largest cluster observed, i.e.

$$N_{\mathrm{tot}} = \sum_{j=2}^{\infty} N_j$$

This definition is consistent with our hypothesis that the formation of dimer is the rate-limiting step of the nucleation process in our experiments.

SUPPLEMENTARY MATERIALS

Supplementary material for this article is available at http://advances.sciencemag.org/cgi/content/full/7/3/eabd9954/DC1

REFERENCES AND NOTES

1. E. M. Dunne, H. Gordon, A. Kürten, J. Almeida, J. Duplissy, C. Williamson, I. K. Ortega, K. J. Pringle, A. Adamov, U. Baltensperger, P. Barmet, F. Benduhn, F. Bianchi, M. Breitenlechner, A. Clarke, J. Curtius, J. Dommen, N. M. Donahue, S. Ehrhart, R. C. Flagan, A. Franchin, R. Guida, J. Hakala, A. Hansel, M. Heinritzi, T. Jokinen, J. Kangasluoma, J. Kirkby, M. Kulmala, A. Kupc, M. J. Lawler, K. Lehtipalo, V. Makhmutov, G. Mann, S. Mathot, J. Merikanto, P. Miettinen, A. Nenes, A. Onnela, A. Rap, C. L. S. Reddington, F. Riccobono, N. A. D. Richards, M. P. Rissanen, L. Rondo, N. Sarnela, S. Schobesberger, K. Sengupta, M. Simon, M. Sipilä, J. N. Smith, Y. Stozkhov, A. Tomé, J. Tröstl, P. E. Wagner, D. Wimmer, P. M. Winkler, D. R. Worsnop, K. S. Carslaw, Global atmospheric particle formation from CERN CLOUD measurements. *Science* **354**, 1119–1124 (2016).
2. H. Gordon, J. Kirkby, U. Baltensperger, F. Bianchi, M. Breitenlechner, J. Curtius, A. Dias, J. Dommen, N. M. Donahue, E. M. Dunne, J. Duplissy, S. Ehrhart, R. C. Flagan, C. Frege, C. Fuchs, A. Hansel, C. R. Hoyle, M. Kulmala, A. Kürten, K. Lehtipalo, V. Makhmutov, U. Molteni, M. P. Rissanen, Y. Stozkhov, J. Tröstl, G. Tsagkogeorgas, R. Wagner, C. Williamson, D. Wimmer, P. M. Winkler, C. Yan, K. S. Carslaw, Causes and importance of new particle formation in the present-day and preindustrial atmospheres. *J. Geophys. Res. Atmos.* **122**, 8739–8760 (2017).
3. P. B. Machado, J. G. Monteiro, J. L. Medeiros, H. D. Epsom, O. Q. Araujo, Supersonic separation in onshore natural gas dew point plant. *J. Nat. Gas Sci. Eng.* **6**, 43–49 (2012).
4. M. Ahmad, M. Casey, N. Sürken, Experimental assessment of droplet impact erosion resistance of steam turbine blade materials. *Wear* **267**, 1605–1618 (2009).
5. T. P. M. Goumans, S. T. Bromley, Efficient nucleation of stardust silicates via heteromolecular homogeneous condensation. *Mon. Not. R. Astron. Soc.* **420**, 3344–3349 (2012).
6. C. N. Jen, P. H. McMurry, D. R. Hanson, Stabilization of sulfuric acid dimers by ammonia, methylamine, dimethylamine, and trimethylamine. *J. Geophys. Res. Atmos.* **119**, 7502–7514 (2014).

7. R. Zhang, I. Suh, J. Zhao, D. Zhang, E. C. Fortner, X. Tie, L. T. Molina, M. J. Molina, Atmospheric new particle formation enhanced by organic acids. *Science* **304**, 1487–1490 (2004).
8. V.-M. Kerminen, X. Chen, V. Vakkari, T. Petäjä, M. Kulmala, F. Bianchi, Atmospheric new particle formation and growth: Review of field observations. *Environ. Res. Lett.* **13**, 103003 (2018).
9. M. Chen, M. Titcombe, J. Jiang, C. Jen, C. Kuang, M. L. Fischer, F. L. Eisele, J. I. Siepmann, D. R. Hanson, J. Zhao, P. H. McMurry, Acid–base chemical reaction model for nucleation rates in the polluted atmospheric boundary layer. *Proc. Natl. Acad. Sci. U.S.A.* **109**, 18713–18718 (2012).
10. A. Määttänen, J. Merikanto, H. Henschel, J. Duplissy, R. Makkonen, I. K. Ortega, H. Vehkamäki, New parameterizations for neutral and ion-induced sulfuric acid-water particle formation in nucleation and kinetic regimes. *J. Geophys. Res. Atmos.* **123**, 1269–1296 (2018).
11. F. Riccobono, S. Schobesberger, C. E. Scott, J. Dommen, I. K. Ortega, L. Rondo, J. Almeida, A. Amorim, F. Bianchi, M. Breitenlechner, A. David, A. Downard, E. M. Dunne, J. Duplissy, S. Ehrhart, R. C. Flagan, A. Franchin, A. Hansel, H. Junninen, M. Kajos, H. Keskinen, A. Kupc, A. Kürten, A. N. Kvashin, A. Laaksonen, K. Lehtipalo, V. Makhmutov, S. Mathot, T. Nieminen, A. Onnela, T. Petäjä, A. P. Praplan, F. D. Santos, S. Schallhart, J. H. Seinfeld, M. Sipilä, D. V. Spracklen, Y. Stozhkov, F. Stratmann, A. Tomé, G. Tsagkogeorgas, P. Vaattovaara, Y. Viisanen, A. Vrtala, P. E. Wagner, E. Weingartner, H. Wex, D. Wimmer, K. S. Carslaw, J. Curtius, N. M. Donahue, J. Kirkby, M. Kulmala, D. R. Worsnop, U. Baltensperger, Oxidation products of biogenic emissions contribute to nucleation of atmospheric particles. *Science* **344**, 717–721 (2014).
12. L. Yao, O. Garmash, F. Bianchi, J. Zheng, C. Yan, J. Kontkanen, H. Junninen, S. B. Mazon, M. Ehn, P. Paasonen, M. Sipilä, M. Wang, X. Wang, S. Xiao, H. Chen, Y. Lu, B. Zhang, D. Wang, Q. Fu, F. Geng, L. Li, H. Wang, L. Qiao, X. Yang, J. Chen, V.-M. Kerminen, T. Petäjä, D. R. Worsnop, M. Kulmala, L. Wang, Atmospheric new particle formation from sulfuric acid and amines in a Chinese megacity. *Science* **361**, 278–281 (2018).
13. G.-L. Hou, W. Lin, X.-B. Wang, Direct observation of hierarchic molecular interactions critical to biogenic aerosol formation. *Commun. Chem.* **1**, 37 (2018).
14. C. Li, R. Signorell, Understanding vapor nucleation on the molecular level: A review. *J. Aerosol Sci.*, 105676 (2020).
15. E. Zapadinsky, M. Passananti, N. Myllys, T. Kurtén, H. Vehkamäki, Modeling on fragmentation of clusters inside a mass spectrometer. *J. Phys. Chem. A* **123**, 611–624 (2019).
16. M. Passananti, E. Zapadinsky, T. Zanca, J. Kangasluoma, N. Myllys, M. P. Rissanen, T. Kurtén, M. Ehn, M. Attoui, H. Vehkamäki, How well can we predict cluster fragmentation inside a mass spectrometer? *Chem. Commun.* **55**, 5946–5949 (2019).
17. J. Zhao, F. L. Eisele, M. Titcombe, C. Kuang, P. H. McMurry, Chemical ionization mass spectrometric measurements of atmospheric neutral clusters using the cluster-CIMS. *J. Geophys. Res. Atmos.* **115**, D08205 (2010).
18. T. Jokinen, M. Sipilä, H. Junninen, M. Ehn, G. Lönn, J. Hakala, T. Petäjä, R. L. Mauldin III, M. Kulmala, D. R. Worsnop, Atmospheric sulphuric acid and neutral cluster measurements using CI-APi-TOF. *Atmos. Chem. Phys.* **12**, 4117–4125 (2012).
19. A. Kürten, T. Jokinen, M. Simon, M. Sipilä, N. Sarnela, H. Junninen, A. Adamov, J. Almeida, A. Amorim, F. Bianchi, M. Breitenlechner, J. Dommen, N. M. Donahue, J. Duplissy, S. Ehrhart, R. C. Flagan, A. Franchin, J. Hakala, A. Hansel, M. Heinritzi, M. Hutterli, J. Kangasluoma, J. Kirkby, A. Laaksonen, K. Lehtipalo, M. Leiminger, V. Makhmutov, S. Mathot, A. Onnela, T. Petäjä, A. P. Praplan, F. Riccobono, M. P. Rissanen, L. Rondo, S. Schobesberger, J. H. Seinfeld, G. Steiner, A. Tomé, J. Tröstl, P. M. Winkler, C. Williamson, D. Wimmer, P. Ye, U. Baltensperger, K. S. Carslaw, M. Kulmala, D. R. Worsnop, J. Curtius, Neutral molecular cluster formation of sulfuric acid–dimethylamine observed in real time under atmospheric conditions. *Proc. Natl. Acad. Sci. U.S.A.* **111**, 15019–15024 (2014).
20. H. Henschel, T. Kurtén, H. Vehkamäki, Computational study on the effect of hydration on new particle formation in the sulfuric acid/ammonia and sulfuric acid/dimethylamine systems. *J. Phys. Chem. A* **120**, 1886–1896 (2016).
21. H. Yu, L. Dai, Y. Zhao, V. P. Kanawade, S. N. Tripathi, X. Ge, M. Chen, S.-H. Lee, Laboratory observations of temperature and humidity dependencies of nucleation and growth rates of sub-3 nm particles. *J. Geophys. Res. Atmos.* **122**, 1919–1929 (2017).
22. J. J. Ferreiro, S. Chakrabarty, B. Schläppi, R. Signorell, Observation of propane cluster size distributions during nucleation and growth in a Laval expansion. *J. Chem. Phys.* **145**, 211907–211907 (2016).
23. S. Chakrabarty, J. J. Ferreiro, M. Lippe, R. Signorell, Toluene cluster formation in laval expansions: Nucleation and growth. *J. Phys. Chem. A* **121**, 3991–4001 (2017).
24. M. Lippe, S. Chakrabarty, J. J. Ferreiro, K. K. Tanaka, R. Signorell, Water nucleation at extreme supersaturation. *J. Chem. Phys.* **149**, 244303 (2018).
25. B. Schläppi, J. H. Litman, J. J. Ferreiro, D. Stapfer, R. Signorell, A pulsed uniform Laval expansion coupled with single photon ionization and mass spectrometric detection for the study of large molecular aggregates. *Phys. Chem. Chem. Phys.* **17**, 25761–25771 (2015).
26. J. Bourgalais, V. Roussel, M. Capron, A. Benidar, A. W. Jasper, S. J. Klippenstein, L. Biennier, S. D. Le Picard, Low temperature kinetics of the first steps of water cluster formation. *Phys. Rev. Lett.* **116**, 113401–113401 (2016).
27. J. H. Litman, B. L. Yoder, B. Schläppi, R. Signorell, Sodium-doping as a reference to study the influence of intracluster chemistry on the fragmentation of weakly-bound clusters upon vacuum ultraviolet photoionization. *Phys. Chem. Chem. Phys.* **15**, 940–949 (2013).
28. M. Fárník, J. Lengyel, Mass spectrometry of aerosol particle analogues in molecular beam experiments. *Mass Spectrom. Rev.* **37**, 630–651 (2018).
29. C. Li, M. Lippe, J. Krohn, R. Signorell, Extraction of monomer-cluster association rate constants from water nucleation data measured at extreme supersaturations. *J. Chem. Phys.* **151**, 094305 (2019).
30. M. Lippe, U. Szczepaniak, G.-L. Hou, S. Chakrabarty, J. J. Ferreiro, E. Chasovskikh, R. Signorell, Infrared spectroscopy and mass spectrometry of CO_2 clusters during nucleation and growth. *J. Phys. Chem. A* **123**, 2426–2437 (2019).
31. J. Krohn, M. Lippe, C. Li, R. Signorell, Carbon dioxide and propane nucleation: The emergence of a nucleation barrier. *Phys. Chem. Chem. Phys.* **22**, 15986–15998 (2020).
32. M. Nachbar, D. Duft, T. P. Mangan, J. C. G. Martin, J. M. C. Plane, T. Leisner, Laboratory measurements of heterogeneous CO_2 ice nucleation on nanoparticles under conditions relevant to the Martian mesosphere. *J. Geophys. Res. Planets* **121**, 753–769 (2016).
33. A. Colaprete, O. B. Toon, Carbon dioxide clouds in an early dense Martian atmosphere. *J. Geophys. Res. Planets* **108**, 5025 (2003).
34. I. K. Ortega, A. Määttänen, T. Kurtén, H. Vehkamäki, Carbon dioxide–water clusters in the atmosphere of Mars. *Comput. Theor. Chem.* **965**, 353–358 (2011).
35. M. Hammer, P. E. Wahl, R. Anantharaman, D. Berstad, K. Y. Lervåg, CO_2 capture from off-shore gas turbines using supersonic gas separation. *Energy Procedia* **63**, 243–252 (2014).
36. B. E. Wyslouzil, C. H. Heath, J. L. Cheung, G. Wilemski, Binary condensation in a supersonic nozzle. *J. Chem. Phys.* **113**, 7317–7329 (2000).
37. S. Lee, R. J. Hoobler, S. R. Leone, A pulsed Laval nozzle apparatus with laser ionization mass spectroscopy for direct measurements of rate coefficients at low temperatures with condensable gases. *Rev. Sci. Instrum.* **71**, 1816–1823 (2000).
38. N. Suas-David, S. Thawoos, A. G. Suits, A uniform flow–cavity ring-down spectrometer (UF-CRDS): A new setup for spectroscopy and kinetics at low temperature. *J. Chem. Phys.* **151**, 244202 (2019).
39. B. R. Rowe, J.-B. Marquette, C. Rebrion, Mass-selected ion–molecule reactions at very low temperatures. The CRESUS apparatus. *J. Chem. Soc., Faraday Trans. 2* **85**, 1631–1641 (1989).
40. B. Hansmann, B. Abel, Kinetics in cold Laval nozzle expansions: From atmospheric chemistry to oxidation of biomolecules in the gas phase. *ChemPhysChem* **8**, 343–356 (2007).
41. D. B. Atkinson, M. A. Smith, Radical-molecule kinetics in pulsed uniform supersonic flows: Termolecular association of OH + NO between 90 and 220 K. *J. Phys. Chem.* **98**, 5797–5800 (1994).
42. P. L. James, I. R. Sims, I. W. M. Smith, M. H. Alexander, M. Yang, A combined experimental and theoretical study of rotational energy transfer in collisions between NO($X^2\Pi_{1/2}$, v = 3, J) and He, Ar and N_2 at temperatures down to 7 K. *J. Chem. Phys.* **109**, 3882–3897 (1998).
43. R. J. Shannon, M. A. Blitz, A. Goddard, D. E. Heard, Accelerated chemistry in the reaction between the hydroxyl radical and methanol at interstellar temperatures facilitated by tunnelling. *Nat. Chem.* **5**, 745–749 (2013).
44. L. Belau, K. R. Wilson, S. R. Leone, M. Ahmed, Vacuum ultraviolet (VUV) photoionization of small water clusters. *J. Phys. Chem. A* **111**, 10075–10083 (2007).
45. B. Schläppi, J. J. Ferreiro, J. H. Litman, R. Signorell, Sodium-sizer for neutral nanosized molecular aggregates: Quantitative correction of size-dependence. *Int. J. Mass spectrom.* **372**, 13–21 (2014).
46. J. H. Seinfeld, S. N. Pandis, *Atmospheric Chemistry and Physics: From Air Pollution to Climate Change* (John Wiley & Sons, ed. 3, 2016).
47. V. deutscher Ingenieure, G. V. und Chemieingenieurwesen, *VDI-Wärmeatlas* (Springer Vieweg, 2013).
48. R. Halonen, E. Zapadinsky, T. Kurtén, H. Vehkamäki, B. Reischl, Rate enhancement in collisions of sulfuric acid molecules due to long-range intermolecular forces. *Atmos. Chem. Phys.* **19**, 13355–13366 (2019).
49. C. M. Lovejoy, D. J. Nesbitt, The infrared spectra of nitrous oxide–HF isomers. *J. Chem. Phys.* **90**, 4671–4680 (1989).
50. J. Troe, Atom and radical recombination reactions. *Annu. Rev. Phys. Chem.* **29**, 223–250 (1978).
51. D. L. Bunker, N. Davidson, On the interpretation of halogen atom recombination rates. *J. Am. Chem. Soc.* **80**, 5090–5096 (1958).
52. K. Luther, K. Oum, J. Troe, The role of the radical-complex mechanism in the ozone recombination/dissociation reaction. *Phys. Chem. Chem. Phys.* **7**, 2764–2770 (2005).
53. S. Aloisio, J. S. Francisco, R. R. Friedl, Experimental evidence for the existence of the HO_2–H_2O complex. *J. Phys. Chem. A* **104**, 6597–6601 (2000).
54. K. Yasuoka, M. Matsumoto, Molecular dynamics of homogeneous nucleation in the vapor phase. I. Lennard-Jones fluid. *J. Chem. Phys.* **109**, 8451–8462 (1998).
55. H. Sabbah, L. Biennier, S. J. Klippenstein, I. R. Sims, B. R. Rowe, Exploring the role of PAHs in the formation of soot: Pyrene dimerization. *J. Phys. Chem. Lett.* **1**, 2962–2967 (2010).

56. M. J. Frisch, G. W. Trucks, H. B. Schlegel, G. E. Scuseria, M. A. Robb, J. R. Cheeseman, G. Scalmani, V. Barone, B. Mennucci, G. A. Petersson, H. Nakatsuji, M. Caricato, X. Li, H. P. Hratchian, A. F. Izmaylov, J. Bloino, G. Zheng, J. L. Sonnenberg, M. Hada, M. Ehara, K. Toyota, R. Fukuda, J. Hasegawa, M. Ishida, T. Nakajima, Y. Honda, O. Kitao, H. Nakai, T. Vreven, J. A. Montgomery, Jr., J. E. Peralta, F. Ogliaro, M. Bearpark, J. J. Heyd, E. Brothers, K. N. Kudin, V. N. Staroverov, T. Keith, R. Kobayashi, J. Normand, K. Raghavachari, A. Rendell, J. C. Burant, S. S. Iyengar, J. Tomasi, M. Cossi, N. Rega, J. M. Millam, M. Klene, J. E. Knox, J. B. Cross, V. Bakken, C. Adamo, J. Jaramillo, R. Gomperts, R. E. Stratmann, O. Yazyev, A. J. Austin, R. Cammi, C. Pomelli, J. W. Ochterski, R. L. Martin, K. Morokuma, V. G. Zakrzewski, G. A. Voth, P. Salvador, J. J. Dannenberg, S. Dapprich, A. D. Daniels, O. Farkas, J. B. Foresman, J. V. Ortiz, J. Cioslowski, D. J. Fox, *Gaussian 09, Revision D.01* (Gaussian Inc., Wallingford CT, 2013).
57. S. Tanimura, Y. Park, A. Amaya, V. Modak, B. E. Wyslouzil, Following heterogeneous nucleation of CO_2 on H_2O ice nanoparticles with microsecond resolution. *RSC Adv.* **5**, 105537–105550 (2015).
58. Y. Park, B. E. Wyslouzil, CO_2 condensation onto alkanes: Unconventional cases of heterogeneous nucleation. *Phys. Chem. Chem. Phys.* **21**, 8295–8313 (2019).
59. I. K. Ortega, N. M. Donahue, T. Kurtén, M. Kulmala, C. Focsa, H. Vehkamäki, Can highly oxidized organics contribute to atmospheric new particle formation? *J. Phys. Chem. A* **120**, 1452–1458 (2016).
60. D. Stolzenburg, L. Fischer, A. L. Vogel, M. Heinritzi, M. Schervish, M. Simon, A. C. Wagner, L. Dada, L. R. Ahonen, A. Amorim, A. Baccarini, P. S. Bauer, B. Baumgartner, A. Bergen, F. Bianchi, M. Breitenlechner, S. Brilke, S. B. Mazon, D. Chen, A. Dias, D. C. Draper, J. Duplissy, I. El Haddad, H. Finkenzeller, C. Frege, C. Fuchs, O. Garmash, H. Gordon, X. He, J. Helm, V. Hofbauer, C. R. Hoyle, C. Kim, J. Kirkby, J. Kontkanen, A. Kürten, J. Lampilahti, M. Lawler, K. Lehtipalo, M. Leiminger, H. Mai, S. Mathot, B. Mentler, U. Molteni, W. Nie, T. Nieminen, J. B. Nowak, A. Ojdanic, A. Onnela, M. Passananti, T. Petäjä, L. L. J. Quéléver, M. P. Rissanen, N. Sarnela, S. Schallhart, C. Tauber, A. Tomé, R. Wagner, M. Wang, L. Weitz, D. Wimmer, M. Xiao, C. Yan, P. Ye, Q. Zha, U. Baltensperger, J. Curtius, J. Dommen, R. C. Flagan, M. Kulmala, J. N. Smith, D. R. Worsnop, A. Hansel, N. M. Donahue, P. M. Winkler, Rapid growth of organic aerosol nanoparticles over a wide tropospheric temperature range. *Proc. Natl. Acad. Sci. U.S.A.* **115**, 9122–9127 (2018).
61. H. Woolley, Thermodynamic functions for carbon dioxide in the ideal gas state. *J. Res. Natl. Bur. Stand.* **52**, 289 (1954).

Acknowledgments: We are very grateful to E. Chasovskikh from our group for help with the maintenance of the experimental setup and to D. Stapfer and M. Steger from our workshops for technical support. **Funding:** Financial support was provided by the Swiss National Science Foundation (SNSF project number 200020-172472) and by ETH Zürich. **Author contributions:** C.L. and R.S. designed the research. C.L., J.K., and M.L. carried out the experiments. C.L., J.K., M.L., and R.S. analyzed the data and discussed the results. C.L. and R.S. wrote the paper. **Competing interests:** The authors declare that they have no competing interests. **Data and materials availability:** All data needed to evaluate the conclusions in the paper are present in the paper and/or the Supplementary Materials. Additional data related to this paper may be requested from the authors.

Submitted 24 July 2020
Accepted 16 November 2020
Published 13 January 2021
10.1126/sciadv.abd9954

Citation: C. Li, J. Krohn, M. Lippe, R. Signorell, How volatile components catalyze vapor nucleation. *Sci. Adv.* **7**, eabd9954 (2021).